

Parameters Sharing Exploration and Hetero-Center based Triplet Loss for Visible-Thermal Person Re-Identification

Haijun Liu and Xiaoheng Tan

Abstract—This paper focuses on the visible-thermal cross-modality person re-identification (VT Re-ID) task, whose goal is to match person images between the daytime visible modality and the nighttime thermal modality. The two-stream network is usually adopted to address the cross-modality discrepancy, the most challenging problem for VT Re-ID, by learning the multi-modality person features. In this paper, we explore how many parameters of two-stream network should share, which is still not well investigated in the existing literature. By well splitting the ResNet50 model to construct the modality-specific feature extracting network and modality-sharing feature embedding network, we experimentally demonstrate the effect of parameters sharing of two-stream network for VT Re-ID. Moreover, in the framework of part-level person feature learning, we propose the hetero-center based triplet loss to relax the strict constraint of traditional triplet loss through replacing the comparison of anchor to all the other samples by anchor center to all the other centers. With the extremely simple means, the proposed method can significantly improve the VT Re-ID performance. The experimental results on two datasets show that our proposed method distinctly outperforms the state-of-the-art methods by large margins, especially on RegDB dataset achieving superior performance, rank1/mAP/mINP 91.05%/83.28%/68.84%. It can be a new baseline for VT Re-ID, with simple but effective strategy.

Index Terms—Visible-thermal person re-identification, cross-modality discrepancy, parameters sharing, hetero-center based triplet loss.

I. INTRODUCTION

PERSON re-identification (Re-ID) can be regarded as a retrieval task, which aims at searching a person of interest from multi disjoint cameras deployed at different locations. It has received increasing interests in computer vision community due to its importance in intelligent video surveillance and criminal investigation applications. Visible-visible Re-ID (VV Re-ID), the most common single-modality Re-ID task, has progressed and achieved high performance in recent years [33].

However, in practical scenarios, a 24-hour intelligent surveillance system, the visible-thermal cross-modality person re-identification (VT Re-ID) problem is frequently encountered. For example, criminals always collect information in the day and execute crimes at night, in which case, the query image may be obtained from the thermal camera (or the infrared camera) during the nighttime, while the gallery images

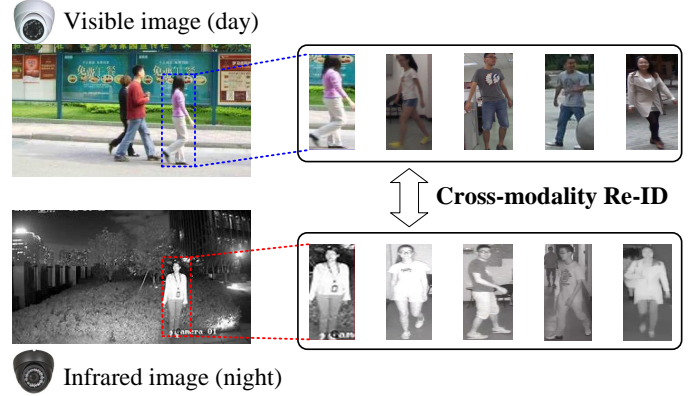


Fig. 1. Illustration of VT Re-ID. For example, searching a person captured by a visible camera in the daytime among multiple persons captured by some infrared (or thermal) cameras at night, and vice versa.

may be captured by the visible cameras during the daytime, as shown in Fig. 1.

In recent years, there are more and more researchers focusing on the VT Re-ID task, achieving big progresses with some novel and effective ideas. However, many works evaluated the effectiveness of their methods with a poor baseline, which seriously impede the development of VT Re-ID community. **In the present study, our proposed method can be set as a strong and effective baseline for VT Re-ID with some extremely simple means.**

The VT Re-ID task suffers from two big problems, the large **cross-modality discrepancy** arisen from the different reflective visible spectrums and sensed emissivities of visible and thermal cameras, and the large **intra-modality variations**, just as the VV Re-ID task, caused by viewpoint changing and different human poses, etc. To alleviate the extra cross-modality discrepancy in VT Re-ID, the intuitive and apparent way is to map the cross-modality persons into a common feature space to realize the similarity measure. Therefore, a two-stream framework is always adopted, including two modality-specific networks with independent parameters for feature extraction, and a parameter-sharing network for feature embedding to project the modality-specific features into a common feature space. Generally speaking, the two modality-specific networks are not required to have the same architecture. The only criterion is that their outputs should be with the same dimension shapes to be the input of parameter-sharing network for feature embedding. In the literature, ResNet50 [7]

model is preferentially adopted as the backbone to construct the two-stream network, all the res-convolution blocks for feature extraction and some parameter-sharing fully-connected layers for feature embedding. However, is this setting the best choice to construct the two-stream network? Those parameter-sharing fully-connected layers can only process the 1D-shaped vector, ignoring the spatial structure information of persons. To take advantage of the convolutional layers for processing the 3D-shaped tensor with spatial structure information, we could share some parameters of res-convolution blocks for feature embedding. In this situation, **how many parameters of two-stream network should share is a point of this study to investigate.**

In addition, the network is always trained with identification loss and triplet loss to simultaneously enlarge the inter-class distance and minimize the intra-class distance. The triplet loss is performed on *each anchor sample to all the other samples* from both the same modality and cross modality. This may be a strong constraint for constraining the pairwise distance of those samples especially when there exist some outliers (bad examples), which would form the adverse triplet to destroy other well learnt pairwise distances. It also will lead to high complexity with large number of triplets. The cross-modality and intra-modality training strategy is separately employed to enhance the feature learning [12], [35]. In my opinion, the separately cross-modality and intra-modality training strategy may be unnecessary, if those learned person features by the two-stream network are good enough in the common feature space, where the features could hardly be distinguished from which modality. **Therefore, we propose the hetero-center based triplet loss directly performing in the unified common feature space.** The hetero-center based triplet loss is performed on *each anchor center to all the other centers*, which also can reduce the computational complexity.

The main contributions can be summarized as follows.

- We achieve the state-of-the-art performance on two datasets by large margins, which can be a strong VT Re-ID baseline to boost the future research with high quality.
- We explore the parameters sharing problem in the two-stream network. To the best of our knowledge, it is the first attempt to analyze the impact of the number of parameters sharing for cross-modality feature learning.
- We propose the hetero-center based triplet loss to constrain the distance of different class centers from both the same modality and cross modality.

II. RELATED WORK

This section will briefly review those existing VT Re-ID approaches. Compared to the traditional VV Re-ID, except the intra-modality variations, VT Re-ID should handle the extra cross-modality discrepancy. To alleviate it, researchers focus on projecting (or translating) the heterogeneous cross-modality person images into a common space for similarity measure, mainly including the following aspects: feature learning, metric learning and image translation.

A. Feature learning

Feature learning is the fundamental step of Re-Identification before similarity measure. Most researches focus on the visible and thermal person feature learning through deep neural networks (DNN). Ye et.al [31], [32], [35] proposed to adopt two-stream network to separately extract the modality-specific features, then perform the feature embedding to project those features into the common feature space with parameters sharing fully connected layers. Based on the two-stream network, Liu et.al [12] introduced the mid-level features incorporation to enhance the modality-shared person features with more discriminability. To learn good modality-shared person features, Dai et.al [2] proposed the cross modality generative adversarial network (cmGAN) under the adversarial learning framework, including a discriminator to distinguish whether the input features are from the visible modality or thermal modality. Zhang et.al [37] proposed a dual-path cross-modality feature learning framework, including a dual-path spatial-structure-preserving common space network and a contrastive correlation network, which preserves intrinsic spatial structures and attends to the difference of input cross-modality image pairs. To explore the potential of both the modality-shared information and the modality-specific characteristics to boost the re-identification performance, Lu et.al [13] proposed to model the affinities of different modality samples according to the shared features and then transfer both shared and specific features among and across modalities.

Moreover, for handling the cross-modality discrepancy, some works concentrate on the input design of single-stream network, to simultaneously utilize the visible and thermal information. Wu et.al [27] firstly proposed to study the VT Re-ID problem, built the SYSU-MM01 dataset, and developed the zero-padding method to extract the modality-shared person features with single-stream network. Kang et.al [9] proposed to combine the visible and thermal images as a single input with different image channels. Additionally, Wang et.al [24] also adopted the multi-spectral image as the input for feature learning, where the multi-spectral image consists of the visible image and corresponding generated thermal image, or the generated visible image and corresponding thermal image.

B. Metric learning

Metric learning is the key step of Re-ID for similarity measure. In deep learning framework, due to the advantage of DNN on feature learning, Re-ID could achieve good performance with only Euclidean distance metric. Therefore, the metric learning is inherent in the training loss function of DNN, guiding the training process to make the extracted features with more discriminate and robust ability. Ye et.al [31] proposed a hierarchical cross-modality matching model by jointly optimizing the modality-specific and modality-shared metrics in a sequential manner. Then, they presented a bi-directional dual-constrained top-ranking loss to learn discriminative feature representations based on two-stream network [35], based on which, the center-constraint is also introduced to improve the performance [32]. Zhu et.al [39] proposed the hetero-center loss to reduce the intra-class cross-modality

variations. Liu et.al [12] also proposed the dual-modality triplet loss to guide the training procedures by simultaneously considering the cross-modality discrepancy and intra-modality variations. Hao et.al [6] proposed an end-to-end two-stream hypersphere manifold embedding network with both classification and identification loss, constraining the intra-modality variations and cross-modality variations on this hypersphere. Zhao et.al [38] introduced the hard pentaplet loss to improve the performance of the cross-modality re-identification. Wu et.al [26] casted the learning shared knowledge for cross-modality matching as the problem of cross-modality similarity preservation, and proposed a focal modality-aware similarity-preserving loss to leverage the intra-modality similarity to guide the inter-modality similarity learning.

C. Image translation

The aforementioned works handle the cross-modality discrepancy and intra-modality variations from the feature extraction level. Recently the image generation methods based on generative adversarial network (GAN) have drawn lots of attention in VT Re-ID, reducing the domain gap between visible and thermal modality from image level. Kniaz et.al [10] firstly introduced GAN to translate a single visible image to a multimodal thermal image set, then performed the Re-ID in the thermal domain. Wang et.al [20] proposed an end-to-end alignment generative adversarial network (AlignGAN) for VT Re-ID, to bridge the cross-modality gap with feature alignment and pixel alignment jointly. Wang et.al [24] proposed dual-level discrepancy reduction learning framework based on a bi-directional cycleGAN to reduce the domain gap, from both the image and feature level. Choi et.al [1] proposed a hierarchical cross-modality disentanglement (Hi-CMD) method, which automatically disentangles ID-discriminative factors and ID-excluded factors from visible-thermal images. Hi-CMD includes an ID-preserving person image generation network and a hierarchical feature learning module.

However, a person in the thermal modality can have different colors of clothes in the visible modality, leading to one thermal person image corresponding to multiple reasonable visible person images by image generation. It is hard to know which one is the correct target to be generated for Re-ID, since when generating images the model can not access the gallery images which only appear in inference phase. The image generation based methods are always with performance uncertainty, high complexity and high training tricks demands.

III. OUR PROPOSED METHOD

In this section, we will introduce the framework of our proposed feature learning model for VT Re-ID, as depicted in Fig. 2. The model mainly consists of three components: (1) the two-stream backbone network, exploring the parameters sharing, (2) the part-level feature extraction block and (3) the loss, our proposed hetero-center based triplet loss and identity softmax loss.

A. Two-stream backbone network

The two-stream network is a conventional way to extract features in visible-thermal cross-modality person re-identification, firstly introduced in [35]. It mainly consists of two parts: feature extractor and feature embedding. Feature extractor aims at learning the modality-specific information from two heterogenous modalities, while the feature embedding focuses on learning the multi-modality shared features for cross-modality re-identification by projecting those modality-specific features into a modality-shared common feature space.

In the existing literature, the feature embedding is always computed by some shared fully connected layers, and the feature extractor is always some well designed convolution neural network, such as ResNet50, etc. In this situation, there may be two problems we should pay attention.

- 1) Feature extractor consists of two branches with independent parameters. If each branch consists of the whole well designed CNN architecture, the number of network parameters (model size) would doubly increases.
- 2) Feature embedding consists of some shared fully connected layers, which can only process the 1D-shaped feature vector without any person spatial structure information. However, the person spatial structure information is crucial to describe a person.

To simultaneously deal with the aforementioned two problems, we propose to split the well designed CNN model into two parts. The former part can be set as two-stream feature extractor with independent parameters, while the latter part can be set as the feature embedding model. In this way, the whole model size will be reduced (corresponding to problem 1). The input of feature embedding block is the output of feature extractor, just the middle 3D feature maps of the well designed CNN model, which is full of the person spatial structure information (corresponding to problem 2).

Therefore, the key point is how to split the well designed CNN model. Namely, how many parameters of the two-stream network should be independent to learn the modality-specific information?

For simplicity in presentation, we denote the visible-stream feature extracting network as function ϕ_v , thermal-stream feature extracting network as ϕ_t to learn the modality-specific information, and the feature embedding network as ϕ_{vt} to project modality-specific person features into the shared common feature space. Given a visible image I_v and a thermal image I_t , the learned 3D person features v and t in common space can be represented as,

$$\begin{cases} v = \phi_{vt}(\phi_v(I_v)), \\ t = \phi_{vt}(\phi_t(I_t)). \end{cases} \quad (1)$$

We will adopt the ResNet50 model as the backbone, with the consideration of its competitive performance in some Re-ID systems as well as its relatively concise architecture. ResNet50 model mainly consists of one shallow convolution block *stage0* and four res-convolution blocks, *stage1*, *stage2*, *stage3* and *stage4*. To split the ResNet50 model into our modality-specific feature extractor and modality-shared feature embedding network, we can sequentially obtained the split

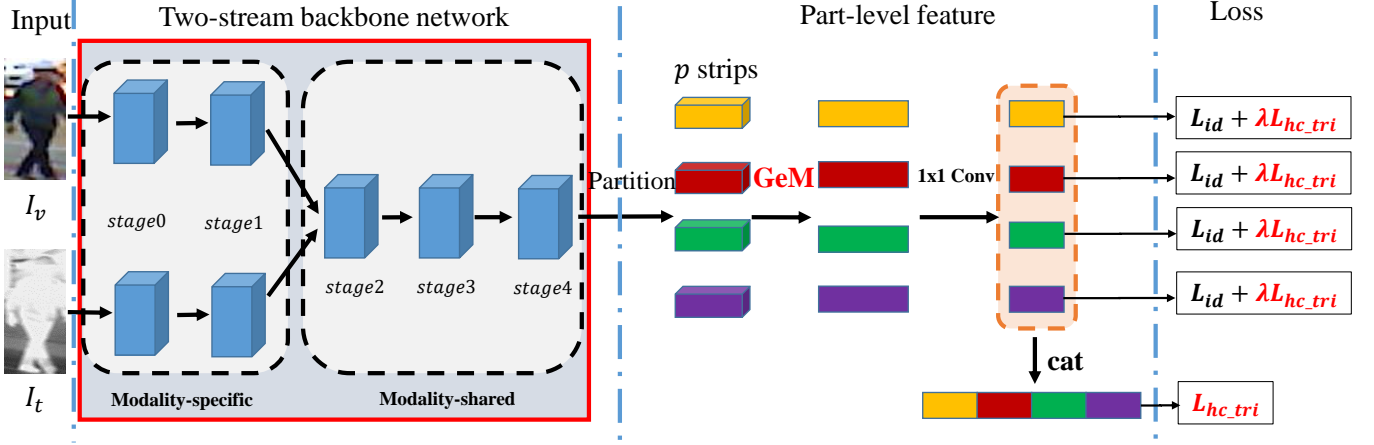


Fig. 2. The pipeline of our proposed framework for VT Re-ID. It mainly contains two components: a two-stream backbone network and the part-level feature learning block. The two-stream backbone network includes two modality-specific branches with independent parameters and following one modality-shared branch with sharing parameters. For example, we take the ResNet50 model as the backbone, the first two stages (*stage0* and *stage1*) forming the modality-specific branches and the following three stages (*stage2*, *stage3* and *stage4*) forming the modality-shared branch. Then, the feature map outputted from the backbone is horizontally split into p 3D tensors, here $p = 4$, which are pooled into vectors by generalized-mean (GeM) pooling operation. For each part vector, a 1×1 Conv block reduces the dimension of features. Afterward, the reduced part features are respectively input to compute the identification loss L_{id} and our proposed hetero-center based triplet loss L_{hc_tri} . Finally, all the part features are concatenated (cat) to form the final person features, which is supervised by L_{hc_tri} .

TABLE I
DIFFERENT SPLITS OF RESNET50 MODEL TO FORM THE TWO-STREAM BACKBONE NETWORK. ϕ_v AND ϕ_t RESPECTIVELY DENOTE THE VISIBLE-STREAM AND THERMAL-STREAM FEATURE EXTRACTING NETWORK. ϕ_{vt} DENOTES THE MODALITY-SHARED FEATURE EMBEDDING NETWORK.

	Modality-specific feature extractor (ϕ_v and ϕ_t)	Modality-shared feature embedding (ϕ_{vt})
$s0$	-	$stage\{0-4\}$
$s1$	$stage\{0\}$	$stage\{1-4\}$
$s2$	$stage\{0-1\}$	$stage\{2-4\}$
$s3$	$stage\{0-2\}$	$stage\{3-4\}$
$s4$	$stage\{0-3\}$	$stage\{4\}$
$s5$	$stage\{0-4\}$	-

scheme as shown in Table I, where $s_i, i = \{0, 1, 2, 3, 4, 5\}$ means ϕ_{vt} starts from the i^{th} stage. $s0$ and $s5$ are two extreme cases. $s0$ means that the two-stream backbone network shares all the ResNet50 model without the modality-specific feature extractor, while $s5$ means that all parameters of the two streams for visible and thermal modality are totally independent just as done in [35]. Which one is the best choice for two-stream backbone network for cross-modality Re-ID? In my opinion, these two extreme cases $s0$ and $s5$ are not good, since they ignore some important information in cross-modality Re-ID task. Experimental results in Sec. IV-B1 show that the modality-shared feature embedding network comprising some res-convolution blocks is a good choice, since the input of modality-shared feature embedding network ϕ_{vt} is 3D shape feature maps, with the spatial structure information of persons.

B. Part-level feature extraction block

In VV Re-ID, the state-of-the-art results are always achieved with part-level deep features [19], [28]. A typical and easy-

going approach is partitioning persons into horizontal strips to coarsely extract the part-level features, which then can be concatenated to describe the person body structure. Body structure is the inherent characteristic of person, which is invariant information of person body whatever modality the image is captured from. Namely, the body structure information is modality-invariant, which could be adopted as modality-shared information to represent a person. Therefore, according to the part-level feature extraction method in [18], [22], we also adopt the uniform partition strategy to obtain coarse body part feature.

Given a person (visible or thermal) images, it will become the 3D feature maps after undergoing all the layers inherited from the two-stream backbone network. Based on the 3D feature maps, as shown in Fig. 2, there are 3 steps to extract the part-level person features as following.

- 1) The 3D feature maps are **uniformly partitioned** into p strips in the horizontal orientation, to generate the coarse body part feature maps, as shown in Fig. 2, where $p = 4$.
- 2) Instead of utilizing the widely-used max-pooling or average-pooling, we adopt a generalized-men (GeM) [16] pooling layer to translate the 3D part feature maps into the 1D part feature vectors. Given a 3D feature patch $X \in R^{C \times H \times W}$, the GeM can be formulated as,

$$\hat{x} = \left(\frac{1}{|X|} \sum_{x_i \in X} x_i^p \right)^{\frac{1}{p}}, \quad (2)$$

where $\hat{x} \in R^{C \times 1 \times 1}$ is the pooled results, $|\cdot|$ denotes the element number, p is the pooling hyperparameter, which can be pre-set or learned by the back-propagating. When $p \rightarrow \infty$ GeM approximates max-pooling, while when $p \rightarrow 1$ GeM approximates average-pooling.

- 3) Afterwards, a 1×1 convolutional (1×1 Conv) block is employed to reduce the dimension of part-level feature

vectors. The block includes a 1×1 convolutional layer whose output channel number is d , following a batch normalization layer and a ReLU layer.

Moreover, each part-level feature vectors are firstly adopted to perform the metric learning with triplet loss L_{tri} (or our proposed hetero-center based triplet loss L_{hc_tri}). Then a fully connected layer with desired dimensions (corresponding to the number of identities of person in our model) is adopted to perform the identification with softmax L_{id} . There are p part-level features that need p different classifiers without sharing parameters.

Finally, all the p part-level features are concatenated (*cat*) to form the final person features for similarity measure during testing. Additionally, the final person features could also be supervised by the L_{tri} (or L_{hc_tri}).

C. The hetero-center based triplet loss

In this subsection, we introduce the designed hetero-center based triplet loss to guide the network training for feature learning. The learning objective is directly conducted in the common feature space to simultaneously deal with both cross-modality discrepancy and intra-modality variations. Firstly, we will revisit the general triplet loss.

1) *Triplet loss revisit*: Triplet loss is firstly proposed in FaceNet [17]. Given an anchor point x_a with class label of y_a , triplet loss aims to make that the positive point x_p belonging to the same class y_a is closer to the anchor than that of a negative point belonging to another class y_n , by at least a margin ρ . Given some pre-selected triplets $\{x_a, x_p, x_n\}$, the triplet loss can be represented as,

$$L_{tri} = \sum_{\substack{a,p,n \\ y_a=y_p \neq y_n}} [\rho + \|x_a - x_p\|_2 - \|x_a - x_n\|_2]_+, \quad (3)$$

where $[x]_+ = \max(x, 0)$ denotes the standard hinge loss, $\|x_a - x_p\|_2$ denotes the Euclidean distance of data point x_a and x_p .

For calculation simplicity and performance improving, Hermans et al. [8] proposed an organizational modification to mine the hard triplets. The core idea is to form batches by randomly sampling P identities, and then randomly sampling K images of each identity, resulting in a mini-batch PK images. For each sample x_a in the mini-batch, we can select the hardest positive and hardest negative samples within the mini-batch to form the triplets for computing the batch hard triplet loss,

$$L_{bh_tri}(X) = \sum_{i=1}^P \sum_{a=1}^K \left[\rho + \underbrace{\max_{p=1 \dots K} \|x_a^i - x_p^i\|_2}_{\text{hardest positive}} - \underbrace{\min_{\substack{j=1 \dots P \\ n=1 \dots K \\ j \neq i}} \|x_a^i - x_n^j\|_2}_{\text{hardest negative}} \right]_+, \quad (4)$$

which is defined for a mini-batch X , where a data point x_a^i denotes the a^{th} image of the i^{th} person in the batch.

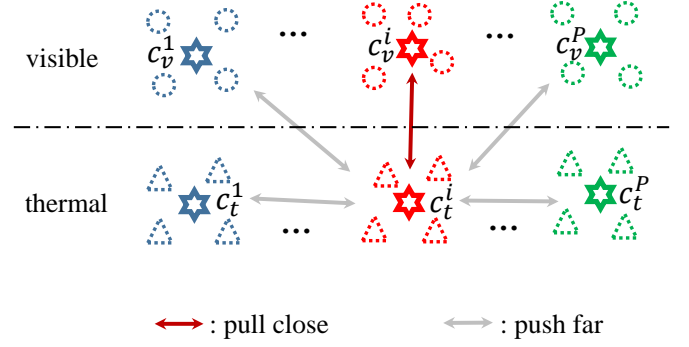


Fig. 3. Illustration of the hetero-center based triplet loss, which aims pulling close those centers with the same identity label from different modalities, while pushing far away those centers with different identity labels no matter which modality it is from. We compare the *center to center similarity* rather than *sample to sample similarity* or *sample to center similarity*. The stars denote the centers. Different colors denote different identities.

2) *Batch sampling method*: Due to our two-stream structure respectively extracting features for visible and thermal images, we introduce the following online batch sampling strategy. Specially, P person identities are firstly randomly selected at each iteration, and then we randomly select K visible images and K thermal images of the selected identity to form the mini-batch, in which totally $2 * PK$ images. This sampling strategy could fully utilize the relationship of all the samples within a mini-batch. In this manner, the sample size of each class is the same, which is important to avoid the perturbations caused by class imbalance. Moreover, due to the randomly sampling mechanism, the local constraint in the mini-batch can achieve the same effect as the global constraint in the entire set.

3) *Hetero-center based triplet loss*: Eq. (4) shows that triplet loss computes the loss by comparison of *anchor to all the other samples*. It is a strong constraint, perhaps too strict to constrain the pairwise distance if there exist some outliers (bad examples), which would form the adverse triplet to destroy other pairwise distance. Therefore, we consider to adopt the center of each person as the identity agent. In this manner, we can relax the strict constraint through replacing the comparison of *anchor to all the other samples* by *anchor center to all the other centers*.

Firstly, in a mini-batch, the center for the features of every identity from each modality is computed,

$$c_v^i = \frac{1}{K} \sum_{j=1}^K v_j^i, \quad (5)$$

$$c_t^i = \frac{1}{K} \sum_{j=1}^K t_j^i,$$

which is defined for a mini-batch, where v_j^i denotes the j^{th} visible image feature of the i^{th} person in the mini-batch, while t_j^i corresponds to the thermal image feature.

Therefore, based on our PK sampling method, in each mini-batch, there would be P visible image centers $\{c_v^i | i = 1, \dots, P\}$ and P thermal centers $\{c_t^i | i = 1, \dots, P\}$, as shown

TABLE II

THE COMPARISON OF COMPUTATIONAL COST BETWEEN GENERAL TRIPLET LOSS L_{bh_tri} AND OUR PROPOSED CENTER-BASED TRIPLET LOSS L_{hc_tri} . DUE TO THE SYMMETRICAL PROPERTY OF DISTANCE MEASURE, THE COMPUTATIONAL COST COULD DIVIDE 2.

	positive	negative
L_{bh_tri}	$2PK \times (2K - 1)$	$2PK \times 2(P - 1)K$
L_{hc_tri}	$2P$	$2P \times 2(P - 1)$

in Fig. 3. In the following, all the computations are only performed on the centers.

The goal of metric learning is to make those features from the same class be close to each other (intra-class compactness), while those features from different classes be far away from each other (inter-class separation). Therefore, in our VT cross-domain Re-ID, based on the PK sampling strategy and calculated centers, we can define the hetero-center based triplet loss as,

$$L_{hc_tri}(C) = \sum_{i=1}^P \left[\rho + \|c_v^i - c_t^i\|_2 - \min_{\substack{n \in \{v,t\} \\ j \neq i}} \|c_v^i - c_n^j\|_2 \right]_+ + \sum_{i=1}^P \left[\rho + \|c_t^i - c_v^i\|_2 - \min_{\substack{n \in \{v,t\} \\ j \neq i}} \|c_t^i - c_n^j\|_2 \right]_+, \quad (6)$$

which is defined on a mini-batch centers C including both visible centers $\{c_v^i | i = 1, \dots, P\}$ and thermal centers $\{c_t^i | i = 1, \dots, P\}$. For each identity, L_{hc_tri} concentrates on the only one cross-modality positive pair, and the mined hardest negative pair in both of the intra and inter modality.

Compared general triplet loss L_{bh_tri} (Eq. (4)) to our proposed center-based triplet loss L_{hc_tri} (Eq. (6)), we replace the comparison of *anchor to all the other samples* by *anchor center to all the other centers*. This modification has two major advantage:

- a) It reduces the computational cost, as shown in Table II. For a mini-batch with $2PK$ images, L_{bh_tri} requires to compute pairwise distance $2PK \times (2K - 1)$ for hardest positive sample mining and $2PK \times 2(P - 1)K$ for hardest negative sample mining. In comparison, L_{hc_tri} only needs to compute the pairwise distance $2P$ for positive sample pairs (there are only P cross-modality positive center pairs), and $2P \times 2(P - 1)$ for hardest negative center sample mining. The computational cost is largely reduced.
- b) It relaxes the sample-based triplet constraint to center-based triplet constraint, which also preserves the property to handle both the intra-class and inter-class variations simultaneously on visible and thermal modalities in the common feature space. On the one hand, for each identity, minimizing the only cross-modality positive center pairwise distance could ensure intra-class feature compactness. On the other hand, the hardest negative center mining could ensure the inter-class feature distinguishable property both in visible and thermal modality.

4) *Comparison to other center-based losses*: There are two kinds of center-based losses: the learned centers [25], [32] and

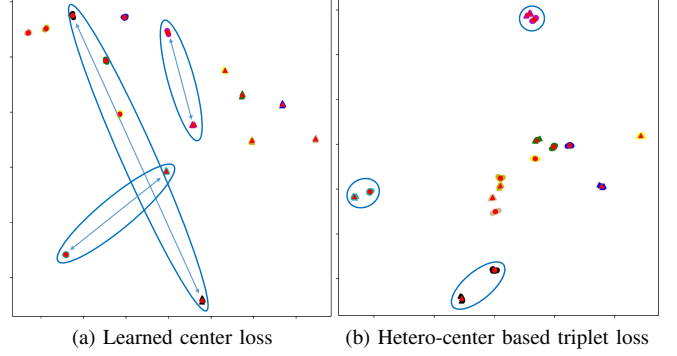


Fig. 4. The visualization of features extracted by the baseline model with (a) the learned center loss and (b) our proposed hetero-center based triplet loss. The features is from 8 random chosen identities in RegDB testing dataset, whose dimension of features is reduced to 2 by tSNE. Points with different colors denote features belonging to different identities. Points of different shapes denote different modalities. The red points with different shapes denote the feature centers of each identity from different modalities. Blue arrows in the blue circles link the two centers of one identity from two modalities.

the computed centers [39]. The main difference lies on the way of obtaining the centers, one is to learn by pre-setting a center parameter for each class, while the other is to compute the centers directly based on the learned deep features.

The learned centers. The learned center loss [25] is firstly introduced in face verification to learn a center for the features of each class and penalizes the distances between the deep features and their corresponding centers. The learned center loss L_{lc} can be formulated as follows,

$$L_{lc} = \frac{1}{2} \sum_{i=1}^P \sum_{j=1}^K \|x_j^i - c^i\|_2, \quad (7)$$

where $c^i \in R^d$ is a d -dimensional parameters to be learned denoting the i^{th} class center.

As to our cross-modality VT Re-ID task with the PK sampling strategy, the learned center loss could be extended into a bi-directional manner [12], [32], [35] as follows,

$$L_{lc} = \frac{1}{2} \sum_{i=1}^P \sum_{j=1}^K (\|v_j^i - c^i\|_2 + \|t_j^i - c^i\|_2), \quad (8)$$

where v_j^i denotes the j^{th} visible image feature of the i^{th} person in the mini-batch, while t_j^i corresponds to the thermal image feature. c^i is the i^{th} class center for both visible and thermal modalities.

Compared the learned center loss L_{lc} (Eq. (8)) to our proposed hetero-center based triplet loss L_{hc_tri} (Eq. (6)), there are the following differences. 1) L_{hc_tri} is in a comparison manner of *anchor center to centers* rather than L_{lc} 's *anchor sample to centers*. 2) L_{hc_tri} respectively computes the center for visible and thermal modalities, while L_{lc} unifies the i^{th} class center for both visible and thermal modalities into one to be learned vector. 3) L_{hc_tri} is formulated in the triplet mining manner with the property of both the inter-class separability and intra-class compactness, while L_{lc} only focuses on the intra-class compactness ignoring the inter-class separability.

As shown in Fig. 4, our proposed hetero-center based triplet loss L_{hc_tri} truly concentrates on both of the inter-class

separability and intra-class compactness, while the learned center loss L_{lc} ignores the inter-class separability for both of the intra and inter modality. L_{lc} only performs well on intra-modality intra-class compactness, however badly on cross-modality intra-class compactness. This maybe due to the hard training of learned center loss combined with identification loss, which leads the unsatisfactory performance.

The computed centers. The other way to obtain the center of each class is to directly calculate based on the learned deep features [39]. We also adopt this manner. Instead of pre-setting a center parameters to be learned as Eq. (7), the centers are directly calculated as Eq. (5). In [39], the hetero-center loss L_{hc} was proposed to improve the intra-class cross-modality similarity, penalizing the center distance between two modality distribution, which can be formulated as follows,

$$L_{hc} = \sum_{i=1}^P \|c_v^i - c_t^i\|_2. \quad (9)$$

Compared the hetero-center loss L_{hc} (Eq. (9)) to our proposed hetero-center based triplet loss L_{hc_tri} (Eq. (6)), the main difference is that, L_{hc} only focuses on the intra-class cross-modality compactness (the red arrows in Fig. 3), while our L_{hc_tri} additionally pay attention to the inter-class separability for both of the intra and inter modality (the grey arrows in Fig. 3) in a triplet mining manner. In summary, L_{hc} is only a part of our proposed L_{hc_tri} .

5) *The overall loss:* Moreover, similar to some state-of-the-art VT Re-ID methods [6], [24], [32], [35], [39], for the sake of feasibility and effectiveness for classification, the identification loss is also utilized to integrate the identity specific information by treating each person as a class. The identification loss with label smooth operation is adopted to prevent from overfitting of training the Re-ID model. Given an image, we denote y as the truth ID label and p_i as the ID prediction logits of the i^{th} class. The identification loss is calculated as follows,

$$L_{id} = \sum_{i=1}^N -q_i \log(p_i) \quad (10)$$

$$s.t. \quad q_i = \begin{cases} 1 - \frac{N-1}{N}\xi, & y = i, \\ \frac{\xi}{N}, & y \neq i, \end{cases}$$

where N is the number of identities in the total training set, ξ is a constant to encourage the model to be less confident on the training set. In this work, ξ is set to be 0.1.

We adopt both of the identification loss and hetero-center based triplet loss for each part-level features, while only the hetero-center based triplet loss $L_{hc_tri}^g$ for the final concatenated global features. Therefore, the final loss is,

$$L_{all} = L_{hc_tri}^g + \sum_{i=1}^p (L_{id}^i + \lambda L_{hc_tri}^i), \quad (11)$$

where λ is a predefined trade-off parameters.

IV. EXPERIMENTS

In this section, we evaluate the effectiveness of our proposed methods to extract the person features for VT Re-ID tasks on



Fig. 5. Illustration of the visible-thermal images, from two datasets SYSU-MM01 [27] and RegDB [15], for cross-modality person re-identification. The first row is the visible images, while the second is the thermal images. Each column contains the images from the same person.

two public datasets, RegDB [15] and SYSU-MM01 [27]. The example images are shown in Fig. 5.

A. Experimental settings

1) *Datasets and settings:* SYSU-MM01 [27] is a large-scale dataset collected by 6 cameras, including 4 visible and 2 infrared cameras, captured in SYSU campus. Some cameras are deployed in the indoor environments and others are deployed in the outdoor environments. The training set contains 395 persons, including 22258 visible images and 11909 infrared images. The testing set contains another 96 persons, including 3803 infrared images for query and 301 randomly selected visible images as gallery set. In *all-search* mode, the gallery set contains all the visible images captured from all four visible cameras. In *indoor-search* mode, the gallery set only contains the visible images captured by two indoor visible cameras. Generally, the all-search mode is more challenging than the indoor-search mode. We exactly follow existing methods to perform 10 trials of the gallery set selection in single-shot setting [32], [35], and then report the average retrieval performance. Details description of the evaluation protocol can be found in [27].

RegDB [15] is constructed by dual-camera (one visible and one thermal camera) systems, and includes 412 persons. For each person, 10 visible images are captured by a visible camera, and 10 thermal images are obtained by a thermal camera. We follow the evaluation protocol in [31] and [35], where the dataset is randomly split into two halves, one for training and the other for testing. For testing, the images from one modality (default is thermal) were used as the gallery set while the ones from the other modality (default is visible) as the probe set. The procedure is repeated for 10 trials to achieve statistically stable results, recording the mean values.

2) *Evaluation Metrics:* Following existing works, cumulative matching characteristics (CMC), mean average precision (mAP) and the mean inverse negative penalty (mINP) are adopted as the evaluation metrics. CMC (Rank-r accuracy) measures the probability of a correct cross-modality person image occurs in the top-r retrieved results. mAP measures the retrieval performance when multiple matching images occur in the gallery set. Moreover, mINP considers the hardest correct

match which determines the workload of inspectors [33]. Note that all the person features are firstly $L2$ normalized for testing.

3) *Implementation details*: The implementation of our method is with Pytorch framework. Following the existing person Re-ID works, ResNet model is adopted as the backbone network for fair comparison, and the pre-trained ImageNet parameters are adopted for the network initialization. Specially, the stride of the last convolutional block is changed from 2 to 1 to obtain fine-grained feature maps with big body size. In training phase, the input images is resized to 288×144 and padded with 10, then randomly left-right flipped and cropped to 288×144 for data augmentation. We adopt the stochastic gradient descent (SGD) optimizer for optimization, and the momentum parameter is set to 0.9. We set the initial learning rate as 0.1 for both datasets. The warmup learning rate strategy is applied to bootstrap the network for enhancing performance. The learning rate (lr) at epoch t is computed as follows,

$$lr(t) = \begin{cases} 0.1 \times \frac{t+1}{10}, & 0 \leq t < 10 \\ 0.1, & 10 \leq t < 20 \\ 0.01, & 20 \leq t < 50 \\ 0.001, & 50 \leq t \end{cases} \quad (12)$$

We set the predefined margin $\rho = 0.3$ for all the triplet losses. For the PK sampling strategy, we set $P = 8$, $K = 4$ for RegDB dataset, and $P = 6$, $K = 8$ for SYSU-MM01 dataset. For the trade-off parameter, we set $\lambda = 2.0$ for RegDB dataset, and $\lambda = 1.0$ for SYSU-MM01 dataset. The dimension of part-level feature d is set to 256 and the number of part-level stripes p is set to 6.

B. Ablation experiments

We evaluate the effectiveness of our proposed method, including three components, two-stream backbone network, part-level feature learning and hetero-center based triplet loss.¹

1) *Two-stream backbone network setting*: As analyzed in Sec. III-A, the key point of two-stream backbone network setting is how to split the well designed CNN model to construct modality-specific feature extractor with independent parameters and the modality-shared feature embedding with shared parameters. Based on the AGW baseline [33] which is designed on top of BagTricks [14], we optionally build the following baseline network with ResNet50 model. As shown in Fig. 6, the 3D feature maps outputted from the two-stream backbone network, are pooled by the generalized-mean pooling (GeM) layer to obtain the 2D feature vector. Then the batch normalization (BN) neck is adopted to train the network, where triplet loss (Eq. (4)) is firstly utilized on the 2D feature vector, then the identification loss is sequentially utilized on the batch normalized feature vector.

The results of different splits of the backbone on RegDB and SYSU-MM01 datasets are listed in Table III, from which we can observe that.

a) $s5$, without sharing any res-convolutional layers, obtains the worst performance on both RegDB and SYSU-MM01

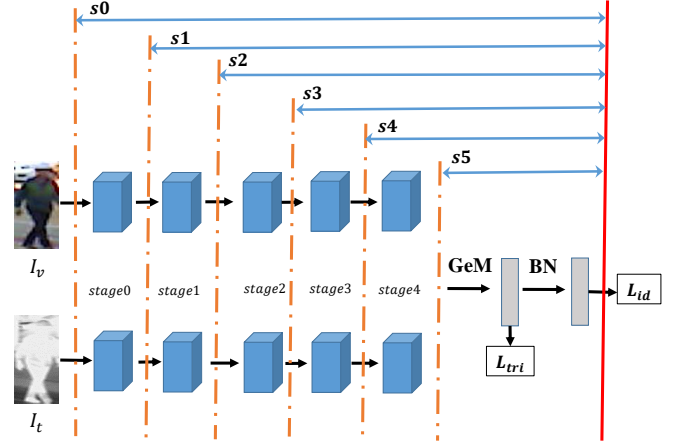


Fig. 6. The illustration of baseline network, mainly illustrating how to split the ResNet50 model to set the two-stream backbone network. $si, i = \{0, 1, 2, 3, 4, 5\}$ denotes that the modality-shared feature embedding block with parameters sharing starts from the i^{th} stage. Then the batch normalization neck with triplet loss and identification loss is adopted to train the network.

TABLE III
THE RESULTS OF DIFFERENT SPLITS OF THE BACKBONE TO FORM THE TWO STREAM NETWORK. $si, i = \{0, 1, 2, 3, 4, 5\}$ DENOTES THAT THE MODALITY-SHARED FEATURE EMBEDDING BLOCK WITH PARAMETERS SHARING STARTS FROM THE i^{th} stage. RE-IDENTIFICATION RATES AT RANK R, MAP AND MINP (%).

splits	r = 1	r = 5	r = 10	r = 20	mAP	mINP
RegDB						
$s0$	77.52	86.50	90.49	93.50	69.79	54.58
$s1$	76.94	85.68	89.71	93.88	69.36	54.82
$s2$	77.14	87.33	91.94	95.19	69.82	54.62
$s3$	76.99	87.23	91.21	94.51	69.51	53.74
$s4$	64.95	78.30	85.00	90.49	60.98	48.62
$s5$	48.93	61.99	71.50	80.44	48.30	37.66
SYSU-MM01						
$s0$	54.38	80.78	88.96	95.06	52.18	38.57
$s1$	54.48	80.38	88.61	94.61	52.67	39.19
$s2$	57.09	81.78	88.80	94.61	54.99	41.26
$s3$	52.20	78.23	86.83	93.06	51.43	39.49
$s4$	45.23	71.50	79.65	88.51	45.43	33.25
$s5$	37.81	69.18	79.88	87.96	39.40	27.68

datasets, with large margins compared to other splits. $s5$ only shares the last fully connected layer to process the 1D feature vector without any person spatial structure information. It demonstrates the effectiveness of the 3D feature maps with person spatial structure information to describe a person.

b) $s0$, sharing all the backbone network, without the modality-specific feature extractor, obtains good performances on both RegDB and SYSU-MM01 datasets. $s0$ equally treats both visible and thermal person images, without paying any extra attention on the color information of visible images, focusing on the spatial structure information of person existing on both visible and thermal images. The results maybe demonstrate that the person spatial structure information is more important compared to the color information in VT cross-modality Re-ID.

¹Note that for simply showing the effectiveness of different components, during the ablation experiments, we only reported the one trial experimental results, rather than the mean results of 10 trials.



Fig. 7. The effect of partition strips p on (a) RegDB and (b) SYSU-MM01 datasets, respectively. Re-identification rates of rank1, mAP and mINP (%).

- c) On RegDB dataset, s_0 , s_1 , s_2 and s_3 achieve comparable performances, while on SYSU-MM01 dataset, s_2 obtains much better Rank1, mAP and mINP results compared to s_0 and s_1 . The different performances maybe come from the different setting of the two datasets. RegDB is collected by a dual-camera system, where the visible image and corresponding thermal image are well aligned, while SYSU-MM01 is collected by 6 disjoint cameras deployed at different locations, where the visible image and corresponding infrared image are with arbitrary poses and views. Therefore, SYSU-MM01 needs more modality-specific layers to extract the person spatial structure compared to RegDB.
- d) Overall, s_2 can achieve the best performance, which only sets *stage0* and *stage1* as the modality-specific feature extractor with acceptable independent parameters.

2) *Part-level feature learning*: To evaluate the effectiveness of part-level feature learning compared to global feature, we add the uniformly partition strategy between the two-stream backbone network and loss layer, as shown in Fig. 2. Based on the above experimental results, we adopt the s_2 split as the two-stream backbone network, still with the supervision of identification loss and triplet loss.

TABLE IV
THE RESULTS OF DIFFERENT POOLING METHODS ON REGDB AND SYSU-MM01 DATASETS, RESPECTIVELY, INCLUDING GENERALIZED-MEAN POOLING (GeM), AVERAGE POOLING (MEAN) AND MAX POOLING (MAX). RE-IDENTIFICATION RATES OF RANK1, MAP AND MINP (%).

Methods	RegDB			SYSU-MM01		
	rank1	mAP	mINP	rank1	mAP	mINP
GeM	85.10	81.40	72.13	57.90	55.10	40.29
Mean	76.75	76.08	68.36	52.09	49.92	35.88
Max	84.22	79.75	69.04	56.74	54.88	40.72

There are three points should pay attention to, 1) the number of partition strips p , 2) the generalized-mean pooling (GeM) layer instead of the traditional average pooling layer or max pooling layer, and 3) the dimension of each part level feature d corresponding to the output channel number of 1×1 Conv.

The effect of partition strips. The number of partition strips determines the granularity of person local feature. Fig. 7 shows the results of different partition strips p on RegDB and SYSU-MM01 datasets. We can observe that 1) the performance of network improves as p increases at first, bigger p corresponds to narrower granularity of local features which leads that the network pays more attention to the detail. 2) However, when p is greater than 6, the performance drops a little (RegDB) or be stable (SYSU-MM01). Maybe it's because that the network could not effectively extract information with such small granularity to obtain a discriminative representation. Moreover, bigger p needs more classifiers with more network parameters. 3) Overall, $p = 6$ is the best setting for partition strips to extract the local person feature.

The effect of GeM. This subsection verify the effectiveness of the generalized-mean pooling (GeM) method compared to the traditional average pooling (Mean) and max pooling (Max) methods. Table IV lists the results of different pooling methods on RegDB and SYSU-MM01 datasets. We can observe that max-pooling performs better than average pooling, while the generalized-mean pooling method performs the best.

The effect of part-level feature dimension. This subsection shows the effect of part-level feature dimension d , corresponding to the output channel number of 1×1 Conv in Fig. 2. The final dimension of person feature is the product of part-level feature dimension d and number of partition strips p . Table V lists the results of different dimensions of each part level feature d on RegDB and SYSU-MM01 datasets. We can find that on SYSU-MM01 dataset $d = 256$ performs the best, while on RegDB dataset $d = 512$ performs the best under rank1 and mAP criteria, $d = 256$ achieves the best performance under mINP criterion. Take both the performance and final person feature dimension into account, we set $d = 256$ for both RegDB and SYSU-MM01 datasets.

3) *Hetero-center based triplet loss*: In this subsection, we verify the effectiveness of our proposed hetero-center based triplet loss L_{hc_tri} from two aspects. On the one hand, L_{hc_tri} is compared to traditional triplet loss L_{bh_tri} to demonstrate the effectiveness of *anchor center to all the other centers* compared to *anchor to all the other samples*. On the other

TABLE V

THE RESULTS OF DIFFERENT DIMENSIONS OF EACH PART LEVEL FEATURE d ON REGDB AND SYSU-MM01 DATASETS, RESPECTIVLY. RE-IDENTIFICATION RATES OF RANK1, MAP AND MINP (%).

d	RegDB			SYSU-MM01		
	rank1	mAP	mINP	rank1	mAP	mINP
128	82.72	79.66	69.96	55.25	53.49	39.36
256	85.10	81.40	72.13	57.90	55.10	40.29
512	86.99	82.02	71.66	57.17	53.89	38.80

TABLE VI

THE EXPERIMENTAL RESULTS OF L_{hc_tri} IS COMPARED TO TRADITIONAL TRIPLET LOSS L_{bh_tri} ON REGDB AND SYSU-MM01 DATASETS, RESPECTIVLY. RE-IDENTIFICATION RATES OF RANK1, MAP AND MINP (%). NOTE THAT L_{bh_tri} LOSS IS NOT CONVERGED ON SYSU-MM01 DATASET WHEN $\lambda \geq 0.5$.

Loss	λ	RegDB			SYSU-MM01		
		rank1	mAP	mINP	rank1	mAP	mINP
L_{bh_tri}	0.1	80.68	75.35	64.50	55.30	54.21	41.09
	0.5	82.43	78.93	69.22	-	-	-
	1.0	85.10	81.40	72.13	-	-	-
	1.5	72.33	69.67	60.55	-	-	-
L_{hc_tri}	0.1	80.73	75.08	64.14	57.53	54.68	40.22
	0.5	87.96	81.97	71.87	60.43	56.41	40.56
	1.0	85.24	81.76	72.33	61.95	57.25	40.44
	1.5	90.63	83.64	71.21	57.45	53.01	36.93
	2.0	92.48	84.41	71.53	-	-	-
	3.0	88.93	78.64	62.22	-	-	-

hand, L_{hc_tri} is compared to the learned center loss L_{lc} and hetero-center loss L_{hc} to demonstrate the effectiveness of constraining both of the inter-class separability and intra-class compactness.

L_{hc_tri} vs. L_{bh_tri} . We conducted experiments under the framework shown in Fig. 2 with different triplet losses, L_{hc_tri} and L_{bh_tri} , fine-tuning the trade-off parameter λ in Eq. (11). The results are listed in Table VI. From the table, we can observe that 1) L_{hc_tri} outperforms L_{bh_tri} on both RegDB and SYSU-MM01 datasets, demonstrating the effectiveness of *anchor center to all the other centers* compared to *anchor to all the other samples*. 2) With the final loss Eq. (11), those non-convergent cases on SYSU-MM01 dataset may show that *anchor to all the other samples* of L_{bh_tri} is truly a strict constraint, demonstrating the effectiveness of the *anchor center to all the other centers* relaxation operation.

L_{hc_tri} vs. L_{lc} and L_{hc} . We conducted experiments with different center based losses, including the learned center loss L_{lc} , hetero-center loss L_{hc} , and our proposed hetero-center based triplet loss L_{hc_tri} . The network is in two manners, the baseline network extracting the global person features (Sec. IV-B1) and the part-level local feature learning network (Sec. IV-B2). The results are listed in Table VII. We can observe that in both two network manners, L_{hc_tri} outperforms L_{lc} and L_{hc} with large margins except the case of baseline network on SYSU-MM01 dataset. It demonstrates the effectiveness of our proposed L_{hc_tri} concentrating on both of the inter-class separability and intra-class compactness, compared to L_{lc} and L_{hc} which only focus on intra-class cross-modality compactness, ignoring the inter-class separability for both of

TABLE VII

THE RESULTS OF DIFFERENT CENTER BASED LOSSES ON REGDB AND SYSU-MM01 DATASETS, RESPECTIVLY, INCLUDING THE LEARNED CENTER LOSS L_{lc} , HETERO-CENTER LOSS L_{hc} , AND OUR PROPOSED HETERO-CENTER BASED TRIPLET LOSS L_{hc_tri} . RE-IDENTIFICATION RATES OF RANK1, MAP AND MINP (%).

Network	Loss	RegDB			SYSU-MM01		
		rank1	mAP	mINP	rank1	mAP	mINP
Baseline	L_{lc}	44.76	40.60	27.52	52.67	50.48	36.84
	L_{hc}	52.96	44.52	27.05	51.30	48.12	33.73
	L_{hc_tri}	72.77	60.89	42.31	54.40	50.72	35.14
Part-level (ours)	L_{lc}	67.38	64.30	54.83	46.02	47.55	36.70
	L_{hc}	85.34	80.83	70.46	47.83	46.22	32.48
	L_{hc_tri}	92.48	84.41	71.53	61.95	57.25	40.44

TABLE VIII

COMPARISON TO THE STATE-OF-THE-ARTS ON REGDB DATASETS IN VISIBLE \rightarrow THERMAL AND THERMAL \rightarrow VISIBLE QUERY SETTINGS. RE-IDENTIFICATION RATES AT RANK R, MAP AND MINP (%).

Methods	Venue	r = 1	r = 10	r = 20	mAP	mINP
Visible \rightarrow Thermal						
Zero-Pad [27]	ICCV17	17.75	34.21	44.35	18.90	-
HCML [31]	AAAI18	24.44	47.53	56.78	20.80	-
HSME [6]	AAAI19	50.85	73.36	81.66	47.00	-
D ² RL [24]	CVPR19	43.40	66.10	76.30	44.10	-
MAC [30]	MM19	36.43	62.36	71.63	37.03	-
AliGAN [20]	ICCV19	57.90	-	-	53.60	-
DFE [5]	MM19	70.13	86.32	91.96	69.14	-
eBDTR [33]	TIFS20	34.62	58.96	68.72	33.46	-
MSR [4]	TIP20	48.43	70.32	79.95	48.67	-
JSIA [21]	AAAI20	48.50	-	-	48.90	-
EDFL [12]	Neuro20	52.58	72.10	81.47	52.98	-
XIV [11]	AAAI20	62.21	83.13	91.72	60.18	-
CDP [3]	Arxiv20	65.00	83.50	89.60	62.70	-
expAT [29]	Arxiv20	66.48	-	-	67.31	-
CMSP [26]	IJCV20	65.07	83.71	-	64.50	-
Hi-CMD [1]	CVPR20	70.93	86.39	-	66.04	-
HAT [34]	TIFS20	71.83	87.16	92.16	67.56	-
cmSSFT [13]	CVPR20	72.30	-	-	72.90	-
MPMN [23]	TMM20	86.56	96.68	98.28	82.91	-
AGW [33]	Arxiv20	70.05	-	-	66.37	50.19
ours	-	91.05	97.16	98.57	83.28	68.84
Thermal \rightarrow Visible						
Zero-Pad [27]	ICCV17	16.63	34.68	44.25	17.82	-
HCML [31]	AAAI18	21.70	45.02	55.58	22.24	-
eBDTR [33]	TIFS20	34.21	58.74	68.64	32.49	-
MAC [30]	MM19	36.20	61.68	70.99	39.23	-
HSME [6]	AAAI19	50.15	72.40	81.07	46.16	-
EDFL [12]	Neuro20	51.89	72.09	81.04	52.13	-
AliGAN [20]	ICCV19	56.30	-	-	53.40	-
expAT [29]	Arxiv20	67.45	-	-	66.51	-
MPMN [23]	TMM20	84.62	95.51	97.33	79.49	-
ours	-	89.30	96.41	98.16	81.46	64.81

the intra and inter modality. It is also illustrated in Fig. 4 through the visualization of features extracted by the baseline model with different center based losses.

C. Comparison to the state-of-the-art

This section conducted the comparison to the state-of-the-art VT Re-ID methods. The results on RegDB and SYSU-MM01

TABLE IX
COMPARISON TO THE STATE-OF-THE-ARTS ON SYSU-MM01 DATASETS. RE-IDENTIFICATION RATES AT RANK R, MAP AND MINP (%).

Methods	Venue	<i>All search</i>					<i>Indoor search</i>				
		r = 1	r = 10	r = 20	mAP	mINP	r = 1	r = 10	r = 20	mAP	mINP
Zero-Pad [27]	ICCV17	14.80	54.12	71.33	15.95	-	20.58	68.38	85.79	26.92	-
cmGAN [2]	IJCAI18	26.97	67.51	80.56	27.80	-	31.63	77.23	89.18	42.19	-
HCML [31]	AAAI18	14.32	53.16	69.17	16.16	-	24.52	73.25	86.73	30.08	-
HSME [6]	AAAI19	20.68	62.74	77.95	23.12	-	-	-	-	-	-
D ² RL [24]	CVPR19	28.90	70.60	82.40	29.20	-	-	-	-	-	-
MAC [30]	MM19	33.26	79.04	90.09	36.22	-	36.43	62.36	71.63	37.03	-
AliGAN [20]	ICCV19	42.40	85.00	93.70	40.70	-	45.90	87.60	94.40	54.30	-
HPILN [38]	TIP19	41.36	84.78	94.51	42.95	-	45.77	91.82	98.46	56.52	-
DFE [5]	MM19	48.71	88.86	95.27	48.59	-	52.25	89.86	95.85	59.68	-
Hi-CMD [1]	CVPR20	34.94	77.58	-	35.94	-	-	-	-	-	-
EDFL [12]	Neuro20	36.94	85.42	93.22	40.77	-	-	-	-	-	-
CDP [3]	Arxiv20	38.00	82.30	91.70	38.40	-	-	-	-	-	-
expAT [29]	Arxiv20	38.57	76.64	86.39	38.61	-	-	-	-	-	-
XIV [11]	AAAI20	49.92	89.79	95.96	50.73	-	-	-	-	-	-
eBDTR [33]	TIFS20	27.82	67.34	81.34	28.42	-	32.46	77.42	89.62	42.46	-
MSR [4]	TIP20	37.35	83.40	93.34	38.11	-	39.64	89.29	97.66	50.88	-
JSIA [21]	AAAI20	38.10	80.70	89.90	36.90	-	43.80	86.20	94.20	52.90	-
CMSP [26]	IJCV20	43.56	86.25	-	44.98	-	48.62	89.50	-	57.50	-
Attri [36]	JEI20	47.14	87.93	94.45	47.08	-	48.03	88.13	95.14	56.84	-
HAT [34]	TIFS20	55.29	92.14	97.36	53.89	-	62.10	95.75	99.20	69.37	-
HC [39]	Neuro20	56.96	91.50	96.82	54.95	-	59.74	92.07	96.22	64.91	-
AGW [33]	Arxiv20	47.50	-	-	47.65	35.30	54.17	-	-	62.97	59.23
ours	-	61.68	93.10	97.17	57.51	39.54	63.41	91.69	95.28	68.17	64.26

datasets are listed in Table VIII and IX, respectively. ²

The experiments on RegDB dataset (Table VIII) demonstrate that our proposed method obtains the best performance in both query setting, always by large margins. We set a new baseline for this dataset, achieving superior performance rank1/mAP/mINP 91.05%/83.28%/68.84% for visible \rightarrow thermal query setting. The experiments suggest that our proposed method can learn better cross-modality sharing features by well designing the two-stream parameter sharing network, learning the part-level local person features, and computing the triplet loss on heterogeneous centers from different modalities.

The experiments on SYSU-MM01 dataset (Table IX) show that our proposed method can achieve comparable performance compared to the current state-of-the-art results obtained by HAT [34], and outperforms all the other comparison methods. However, in the more challenging mode *all-search*, our method performs much better than HAT [34] in the two key criteria rank1/mAP, 61.68%/57.51 vs. 55.29%/53.89%.

Compared to AliGAN [20], D²RL [24] and Hi-CMD [1], our method achieves much better performance on both datasets, and doesn't need the sophisticated cross-modality image translation operation. Meanwhile, our method also doesn't need the complicated adversarial learning with much tricks which is always hard for training.

V. CONCLUSIONS

This paper aims at enhancing the discriminative person feature learning through simple means for VT Re-ID. On the one hand, we explore the parameters sharing settings in the two-stream network. The experimental results show that the modality-sharing feature embedding network with

some convolution blocks is an effective strategy, which could process the 3D shape feature maps with the spatial structure of person. On the other hand, we propose the hetero-center based triplet loss to improve the traditional triplet loss for VT Re-ID, by replacing the comparison of *anchor to all the other samples* by *anchor center to all the other centers*. With the part-level person feature learning, hetero-center based triplet loss performs much better than traditional triplet loss. The experimental results with remarkable improvements on two VT Re-ID datasets demonstrate the effectiveness of our proposed method compared to the current state-of-the-art. Our method with simple but effective strategy can be a strong VT Re-ID baseline to boost the future research with high quality.

REFERENCES

- [1] S. Choi, S. Lee, Y. Kim, T. Kim, and C. Kim, "Hi-cmd: Hierarchical cross-modality disentanglement for visible-infrared person re-identification," in *CVPR*, 2020, pp. 10 257–10 266.
- [2] P. Dai, R. Ji, H. Wang, Q. Wu, and Y. Huang, "Cross-modality person re-identification with generative adversarial training," in *IJCAI*, 2018, pp. 677–683.
- [3] X. Fan, H. Luo, C. Zhang, and W. Jiang, "Cross-spectrum dual-subspace pairing for rgb-infrared cross-modality person re-identification," *arXiv preprint arXiv:2003.00213*, 2020.
- [4] Z. Feng, J. Lai, and X. Xie, "Learning modality-specific representations for visible-infrared person re-identification," *IEEE TIP*, vol. 29, pp. 579–590, 2020.
- [5] Y. Hao, N. Wang, X. Gao, J. Li, and X. yu Wang, "Dual-alignment feature embedding for cross-modality person re-identification," in *ACM MM*, 2019.
- [6] Y. Hao, N. Wang, J. Li, and X. Gao, "Hsme: Hypersphere manifold embedding for visible thermal person re-identification," in *AAAI*, 2019, pp. 8385–8392.
- [7] K. He, X. Zhang, S. Ren, and J. Sun, "Deep residual learning for image recognition," in *CVPR*, 2016, pp. 770–778.
- [8] A. Hermans, L. Beyer, and B. Leibe, "In defense of the triplet loss for person re-identification," *arXiv preprint arXiv:1703.07737*, 2017.

²Note that in this subsection we reported the mean results of 10 trials following the standard dataset settings.

- [9] J. K. Kang, T. M. Hoang, and K. R. Park, "Person re-identification between visible and thermal camera images based on deep residual cnn using single input," *IEEE Access*, vol. 7, pp. 57 972–57 984, 2019.
- [10] V. V. Kniaz, V. A. Knyaz, J. Hladuvka, W. G. Kropatsch, and V. Mizginov, "Thermalgan: Multimodal color-to-thermal image translation for person re-identification in multispectral dataset," in *ECCV Workshops*, 2018.
- [11] D.-G. Li, X. Wei, X. Hong, and Y. Gong, "Infrared-visible cross-modal person re-identification with an x modality," in *AAAI*, 2020.
- [12] H. Liu, J. Cheng, W. Wang, Y. Su, and H. Bai, "Enhancing the discriminative feature learning for visible-thermal cross-modality person re-identification," *Neurocomputing*, vol. 398, pp. 11–19, 2020.
- [13] Y. Lu, Y. Wu, B. Liu, T. Zhang, B. Li, Q. Chu, and N. Yu, "Cross-modality person re-identification with shared-specific feature transfer," in *CVPR*, 2020, pp. 13 379–13 389.
- [14] H. Luo, W. Jiang, Y. Gu, F. Liu, X. Liao, S. Lai, and J. Gu, "A strong baseline and batch normalization neck for deep person re-identification," *IEEE TMM*, pp. 1–1, 2019.
- [15] D. Nguyen, H. Hong, K. Kim, and K. Park, "Person recognition system based on a combination of body images from visible light and thermal cameras," *Sensors*, vol. 17, no. 3, p. 605, 2017.
- [16] F. Radenović, G. Tolias, and O. Chum, "Fine-tuning cnn image retrieval with no human annotation," *IEEE TPAMI*, vol. 41, no. 7, pp. 1655–1668, 2018.
- [17] F. Schroff, D. Kalenichenko, and J. Philbin, "Facenet: A unified embedding for face recognition and clustering," in *CVPR*, 2015, pp. 815–823.
- [18] Y. Sun, L. Zheng, Y. Yang, Q. Tian, and S. Wang, "Beyond part models: Person retrieval with refined part pooling (and a strong convolutional baseline)," in *ECCV*, 2018, pp. 501–518.
- [19] C. Wan, Y. Wu, X. Tian, J. Huang, and X. Hua, "Concentrated local part discovery with fine-grained part representation for person re-identification," *IEEE TMM*, vol. 22, no. 6, pp. 1605–1618, 2020.
- [20] G. Wang, T. Zhang, J. Cheng, S. Liu, Y. Yang, and Z. Hou, "Rgb-infrared cross-modality person re-identification via joint pixel and feature alignment," in *ICCV*, 2019, pp. 3623–3632.
- [21] G. Wang, T. Zhang, Y. Yang, J. Cheng, J. Chang, X. Liang, and Z. Hou, "Cross-modality paired-images generation for rgb-infrared person re-identification," in *AAAI*, 2020.
- [22] G. Wang, Y. Yuan, X. Chen, J. Li, and X. Zhou, "Learning discriminative features with multiple granularities for person re-identification," in *ACM MM*, 2018, pp. 274–282.
- [23] P. Wang, Z. Zhao, F. Su, Y. Zhao, H. Wang, L. Yang, and Y. Li, "Deep multi-patch matching network for visible thermal person re-identification," *IEEE TMM*, pp. 1–1, 2020.
- [24] Z. Wang, Z. Wang, Y. Zheng, Y.-Y. Chuang, and S. Satoh, "Learning to reduce dual-level discrepancy for infrared-visible person re-identification," in *CVPR*, 2019, pp. 618–626.
- [25] Y. Wen, K. Zhang, Z. Li, and Y. Qiao, "A discriminative feature learning approach for deep face recognition," in *ECCV*, 2016.
- [26] A. Wu, W.-S. Zheng, S. Gong, and J. Lai, "Rgb-ir person re-identification by cross-modality similarity preservation," *IJCV*, vol. 128, pp. 1765–1785, 2020.
- [27] A. Wu, W.-S. Zheng, H.-X. Yu, S. Gong, and J. Lai, "Rgb-infrared cross-modality person re-identification," in *ICCV*, 2017, pp. 5380–5389.
- [28] F. Yang, K. Yan, S. Lu, H. Jia, D. Xie, Z. Yu, X. Guo, F. Huang, and W. Gao, "Part-aware progressive unsupervised domain adaptation for person re-identification," *IEEE TMM*, pp. 1–1, 2020.
- [29] H. Ye, H.-C. Liu, F. Meng, and X. Li, "Bi-directional exponential angular triplet loss for rgb-infrared person re-identification," *arXiv preprint arXiv:2006.00878*, 2020.
- [30] M. Ye, X. Lan, and Q. Leng, "Modality-aware collaborative learning for visible thermal person re-identification," in *ACM MM*, 2019.
- [31] M. Ye, X. Lan, J. Li, and P. C. Yuen, "Hierarchical discriminative learning for visible thermal person re-identification," in *AAAI*, 2018.
- [32] M. Ye, X. Lan, Z. Wang, and P. C. Yuen, "Bi-directional center-constrained top-ranking for visible thermal person re-identification," *IEEE TIFS*, vol. 15, pp. 407–419, 2020.
- [33] M. Ye, J. Shen, G. jie Lin, T. Xiang, L. Shao, and S. C. H. Hoi, "Deep learning for person re-identification: A survey and outlook," *arXiv preprint arXiv:2001.04193*, 2020.
- [34] M. Ye, J. Shen, and L. Shao, "Visible-infrared person re-identification via homogeneous augmented tri-modal learning," *IEEE TIFS*, 2020.
- [35] M. Ye, Z. Wang, X. Lan, and P. C. Yuen, "Visible thermal person re-identification via dual-constrained top-ranking," in *IJCAI*, 2018, pp. 1092–1099.
- [36] S. Zhang, C. Chen, W. Song, and Z. Gan, "Deep feature learning with attributes for cross-modality person re-identification," *Journal of Electronic Imaging*, vol. 29, no. 3, 2020.
- [37] S. Zhang, Y. Yang, P. Wang, X. Zhang, and Y. Zhang, "Attend to the difference: Cross-modality person re-identification via contrastive correlation," *arXiv preprint arXiv:1910.11656*, 2019.
- [38] Y.-B. Zhao, J.-W. Lin, Q. Xuan, and X. Xi, "Hpiln: a feature learning framework for cross-modality person re-identification," *IET Image Processing*, vol. 13, no. 14, pp. 2897–2904, 2019.
- [39] Y. Zhu, Z. Yang, L. Wang, S. Zhao, X. Hu, and D. Tao, "Hetero-center loss for cross-modality person re-identification," *Neurocomputing*, vol. 386, pp. 97–109, 2019.